URTeC: 2902311

Downhole Microseismic Mapping of More Than 400 Fracturing Stages on a Multiwell Pad at the Hydraulic Fracturing Test Site (HFTS): Discussion of Operational Challenges and Analytic Results

Neil Stegent*[1] and Cody Candler[1];
1. Pinnacle, A Halliburton Service.

Abstract

The United States Department of Energy co-funded a joint industry project (JIP) in the Midland basin of Texas. The project was conducted in the Wolfcamp formation to better understand the relationships among horizontal lateral placement, production interference between laterals, effectiveness of completion sequences, and hydraulic fracture geometry in unconventional reservoirs. Downhole microseismic data was acquired from more than 400 fracturing stages during the completion project to better understand the generated hydraulic fracture geometries.

Eleven horizontal wells were drilled in the upper Wolfcamp (UW) and middle Wolfcamp (MW) formation in the Permian Basin. The 10,000-ft laterals were drilled in a chevron pattern to help improve inter-well fracture communication and maximize hydrocarbon recovery. The completions sequences were planned to restrain fracture height growth upward into a lower-pressure zone using a combination of zipper fracturing and simultaneous fracturing operations. Downhole microseismic monitoring was used to record more than 95% of the planned fracture stages. Downhole tiltmeters were also used to validate upward fracture height growth. Multiple geophone arrays, both vertical and horizontal, were used during this completion; this paper discusses coordination between maintaining completion efficiency and obtaining microseismic data. Additionally, this paper highlights the completion challenges associated with collecting diagnostic data along with results and findings.

Introduction

The project primarily consisted of 11 horizontal wells drilled in the UW and MW formation in the Midland basin of West Texas. The wells were drilled in a chevron pattern **(Figure 1)** ~660 ft apart laterally and ~450 ft apart diagonally. This configuration can also be called a “wine-rack” or simply a “staggered” pattern. A 5 1/2-in. steel casing was cemented along the entire length of each lateral monobore well. Multiple drilling rigs were used to accomplish this task, and the wellheads resided on three separate physical pads to expedite the drilling process as well as accentuate the completion strategy with multiple fracture spreads. The subsurface laterals were drilled between existing vintage vertical wellbores, most of which were completed in multiple horizons ranging from the Cline to the Spraberry formation.

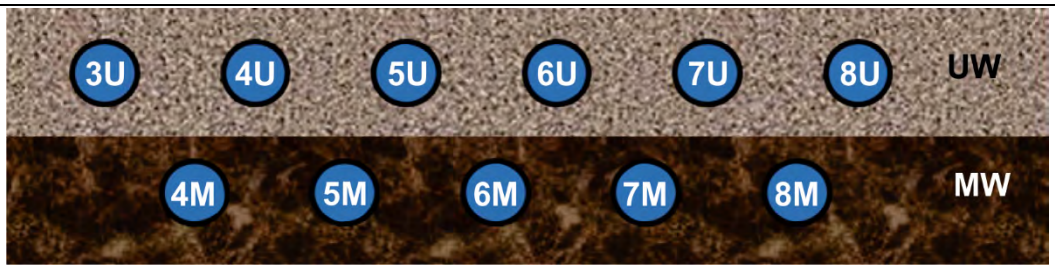

Figure 1: Illustration of chevron well pattern (end view).

The Wolfcamp formation is a combination of quartz and calcite with typical clay content in the 15 to 40% range. It contains thin limestone layers that lie between the UW and lower Wolfcamp (LW) formation and tend to function as weak fracture barriers between the two intervals. The Wolfcamp formation contains natural fractures and matrix permeability in the nano-darcys. The entire Wolfcamp formation section primarily lies between the Spraberry/Dean and the Canyon/Strawn formations. The UW formation is approximately 350-ft thick with an approximately 0.51-psi/ft reservoir pressure gradient and a permeability range of 200 to 800 nano-darcys. The MW formation is approximately 250-ft thick with a slightly higher reservoir pressure gradient (0.53 psi/ft) and a permeability range similar to the UW formation. The Spraberry formation, which lies above the UW formation, tends to be normally pressured or can be slightly higher than the normal reservoir pressure gradient (0.48 psi/ft). The reduction in reservoir pressure results in lower minimum horizontal in-situ formation stress; consequently, fractures tend to extend upward from the UW into the Spraberry formation. This phenomenon has been observed by other operators in the basin and is well documented in the literature [1], [2].

Microseismic Fracture Mapping Project Objectives

Microseismic data provide engineering knowledge for future field developments in this project area as well as in similar unconventional systems. Understanding hydraulic fracture generation in shale reservoirs can help enable the design and execution of effective fracturing stages that significantly contribute to increased hydrocarbon recovery. Improved design and execution could thereby reduce the number of future wells drilled, reduce resource requirements for fracturing, minimize or eliminate potential environmental impacts, and reduce energy input and cost.

The primary fracture mapping objectives during this project were as follows:

- Determine the extent of reservoir coverage from the hydraulic fractures
- Measure fracture or fracture network geometry (i.e., height, length, and width) and azimuth
- Characterize, if possible, the relationship between time (i.e., injected volume) and created fracture half-length and height
- Identify and determine the extent of any interaction with the following:
  - Large-scale, pre-stressed natural geological features
  - Previously produced or stimulated offset vertical wells
- Evaluate the effectiveness and impact of the following on overall fracture geometry:
  - Laterals drilled in the UW and MW using a chevron pattern
  - Zipper fracturing sequence and timing between stages
  - Completing the UW wells before the MW wells
  - Different numbers of fracture initiation points per fracturing stage
- Use downhole microdeformation monitoring to determine the shallowest depth at which fractures could have propagated
- Examine the microseismic data relative to the slant well core intervals

Project Plan and Setup

Downhole microseismic mapping (MSM) data was obtained to better understand the hydraulic fracture systems generated and the hydrocarbon contribution of the natural fracture system of the source rock reservoir. Dual arrays of geophones were used throughout the completion process to acquire the data. **Figure 2** shows the subsurface configuration of all the project wells, with the 11 horizontal wells in the center being the primary test wells. A

downhole hybrid array of geophones and tiltmeters was installed in a vertical well (VM1) that was located in the southeast quadrant of the project pad. The downhole tilts independently measured potential upward fracture growth into the upper Spraberry formation. Downhole tiltmeters measure the actual microdeformation of the rock generated from a hydraulic fracture, which is different from the shear events that are measured with microseismic technology. The bottom of the vertical geophone toolstring array was approximately 1,550 ft above the shallowest lateral. Typically, the array would be installed closer to the formation being fractured. However, because all of the available vertical wellbores had existing perforations, which needed to be plugged back to minimize background noise, Well VM1 was selected because it would allow for the deepest deployment of the vertical geophone array. A second geophone array was tractored into the horizontal lateral of Well 5M and was repositioned during the completion process to remain close to the current treatment application. MSM data acquisition was divided into three phases to accommodate repositioning of geophone arrays (in the vertical wellbores) and maintain high-quality data. The vertical section of some of the horizontal treatment wells was also used for geophone arrays during the different completion phases. Appendix B discusses the MSM quality assurance (QA) process.

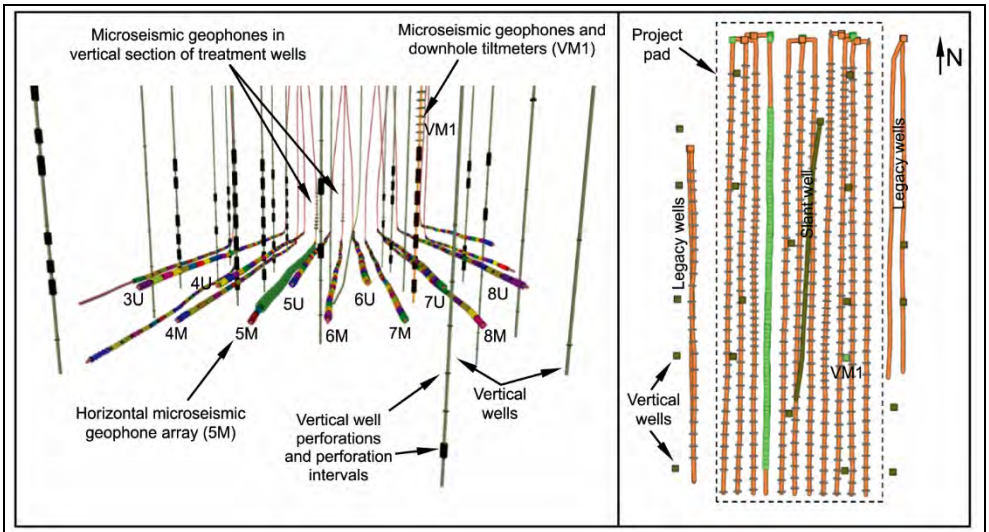

Figure 2: Three-dimensional (3D) and two-dimensional (2D) views of the subsurface project wells.

Previously produced vertical wells are dispersed throughout the project well locations. **Figure 3** shows the publicly recorded cumulative produced volumes of the offset active wells when the 11 wells were completed. A reduction in reservoir pressure also decreases the in-situ stress in a given formation, which can influence the fracture geometry. Depletion can result in asymmetric fracture development and affect fracture containment. Determining the location of areas that might be affected by pressure drawdown is an important consideration during the microseismic data evaluation. **Figure 4** shows a map view of the project area and illustrated historic drainage area.

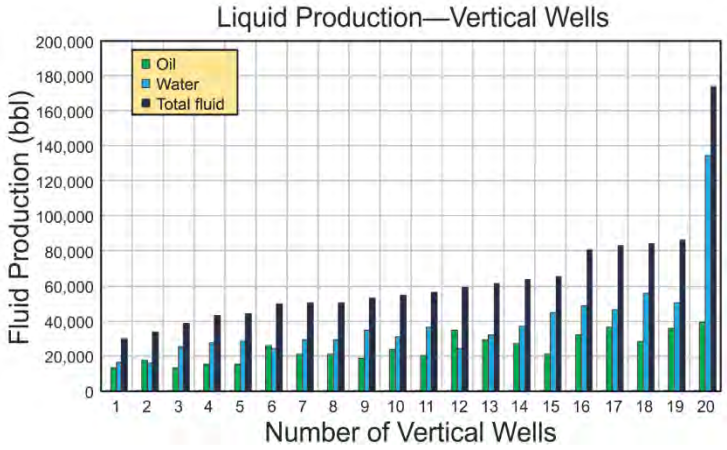

Figure 3: Offset well production.

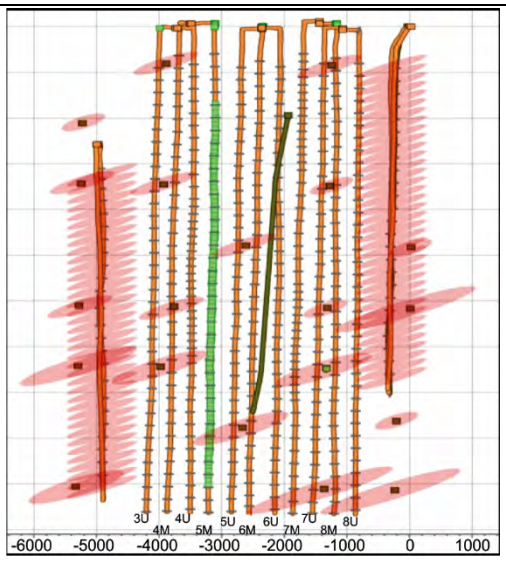

Figure 4: Project wells and existing wellbores (drainage patterns are shown for illustration only).

Approximately 434 fracturing stages were monitored using a dual-array configuration on most of the completions. To maximize the listening distance, the arrays were moved throughout the project completion process. A fracture-mapping hybrid array, which has both MSM geophones and downhole tilt tools configured in the same tool string, was positioned in Well VM1 (vertical). A second horizontal MSM array was deployed into Well 5M (horizontal). Most stages were monitored from this horizontal array, and the array was pulled into the vertical section for the later-stage completions. The last pad well was monitored using two downhole microseismic vertical receiver arrays. Tiltmeters in the hybrid array were fully functional for the duration of the hybrid array use in Well VM1. The bottom tiltmeter was located approximately 1,550 ft above the highest landed treatment lateral and did not detect sufficient microdeformation for a quantifiable diagnostic analysis. **Figure 5** shows the monitoring setup.

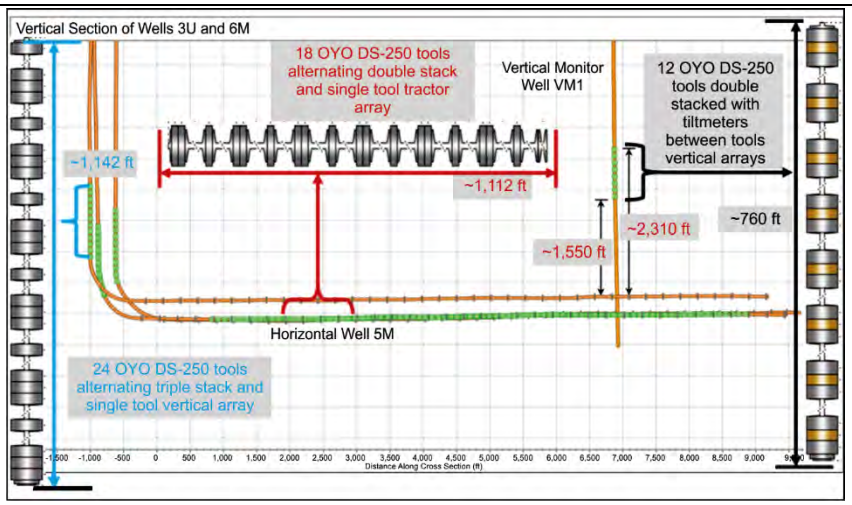

Figure 5: Geophone and tiltmeter arrays.

Well Completion and Fracturing Sequence

Before the completion of the 11-well pad, two offset legacy (parent) wells, located to the east of the project wells, were refractured to repressurize the reservoir (i.e., increase the reservoir stress) and minimize the generation of asymmetric fractures from the development (child) wells. Courtier et al. [3] discuss the refracturing results.

All 11 wells were completed in a similar manner with a high-rate water fracturing treatment containing a friction reducer and a low concentration of surfactant. In addition, a friction reducer breaker was included. The injection rate was designed for 95 bbl/min on both the UW and LW completions. During the design phase, testing of some high-viscosity fluid systems was considered, but it was decided that because of the project complexity, it would be extremely difficult to make significant conclusions based on the completion fluid type. The number of fracturing stages per wellbore ranged from 37 to 49 and spanned ±200 ft/stage. A total of 434 fracturing stages was performed in less than 7 weeks. The number of fracture entry points also alternated between three and five perforation clusters per fracturing stage over a 1 1/2-ft interval. Perforation cluster design varied (number of entry points, spacing between clusters, etc.) on some of the wells to determine the effect of cluster spacing and number of entry points during the completion. A 40/70-mesh proppant was pumped at a total volume equivalent to 1,100 lbm/ft of lateral completed per stage on most wells; however, several wells were completed with proppant volumes equivalent to between 1,400 and 1,800 lbm/ft of lateral completed per stage. Such configurations and fluid systems are typical for the Wolfcamp formation completions in the basin.

A zipper fracturing completion strategy was applied on the 11-well pad using two fracturing crews. Because the in-situ stress decreases between the Spraberry and Wolfcamp formations, the completions were sequenced to minimize upward fracture growth by completing the UW wells before the MW wells. This completion sequence was designed to contain the fracture height development in the MW by increasing the stress in the UW during the completions process. The completion design was also intended to maximize the effective stimulated area of fracture contact or the stimulated reservoir volume (SRV) [4].

The completion plan development required a significant amount of time-consuming complex operational pre-fracture planning and field coordination by the operator and service companies collaborating. Many man-hours were necessary to develop and revise the completion sequence **(Figure 6).**

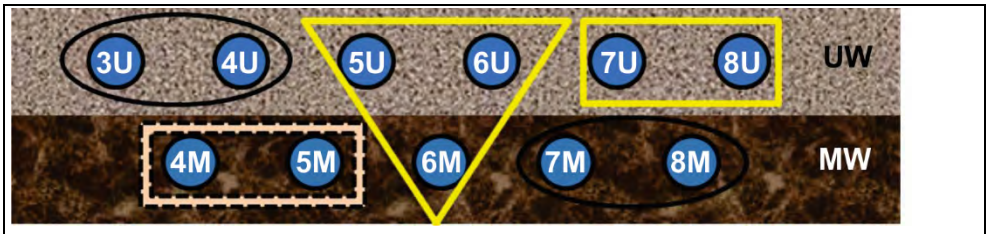

Figure 6: Zipper fracturing completions sequence: Phase 1 (Fracturing Crew 1), Wells 7U and 8U (yellow square); Phase 1 (Fracturing Crew 2), Wells 5U, 6U, and 6M (yellow triangle); Phase 2 (Fracturing Crew 1), Wells 7M and 8M (black oval); Phase 2 (Fracturing Crew 2), Wells 3U and 4U (black oval); Phase 3 (Fracturing Crew 2), Wells 4M and 5M (black dotted square).

The sequencing of the zipper fracturing completion was one of the most efficient and effective project components. Some wells were completed by sequentially completing the first five fracturing stages on one well before beginning the zipper fracturing sequencing on the neighboring lateral, while other sets of wells were completed using alternating sequencing between wells at the beginning of the completion process. An expectation of this design of experiment (DOE) was implemented to determine whether a noticeable difference, with respect to the microseismic measurements, could be correlated to the development of complexity during stimulation. The real-time downhole MSM clearly indicated that the target reservoirs were well stimulated **(Figure 7 and Figure** 8**). Figure 9** shows moderate-to-high fracture height containment in the higher stressed MW horizon with minimal growth up into the UW. The operator of the properties used careful planning with regards to the lateral landing depths of the wells and used in-depth reservoir understanding to improve the likelihood of a successful completion. Appendix A presents MSM examples of individual representative fracturing stages and treatment data with corresponding microseismic measurements.

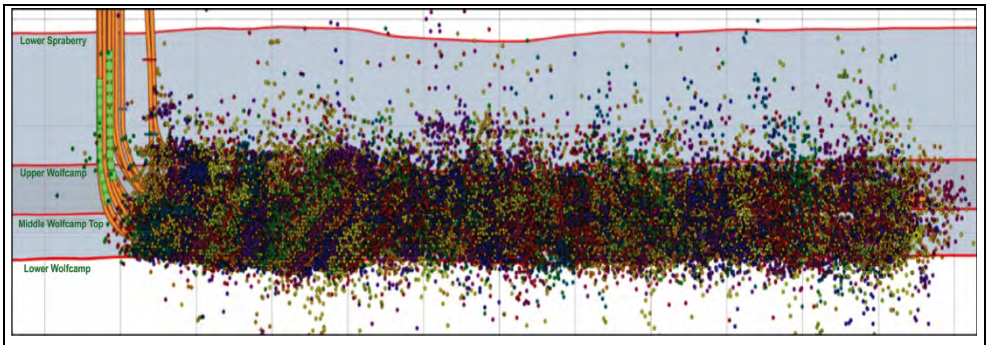

Figure 7: Side view of all real-time microseismic events (colored by fracturing stage).

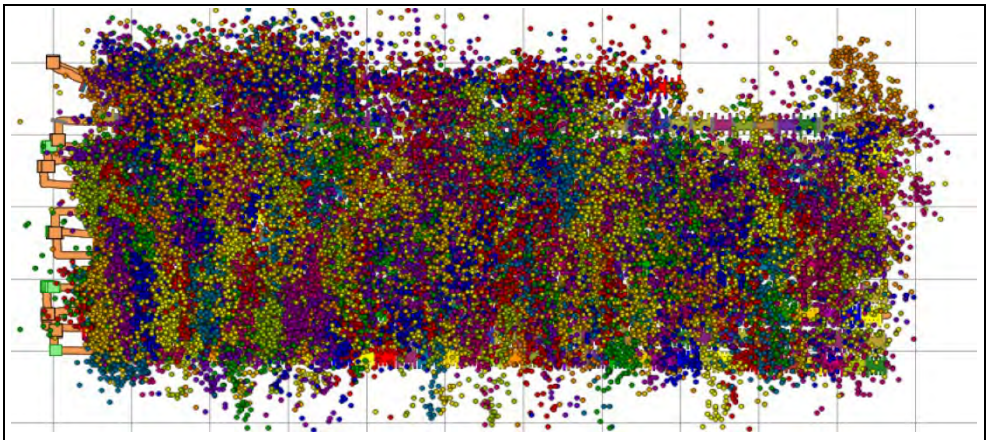

Figure 8: Map view of all real-time microseismic events (colored by fracturing stage).

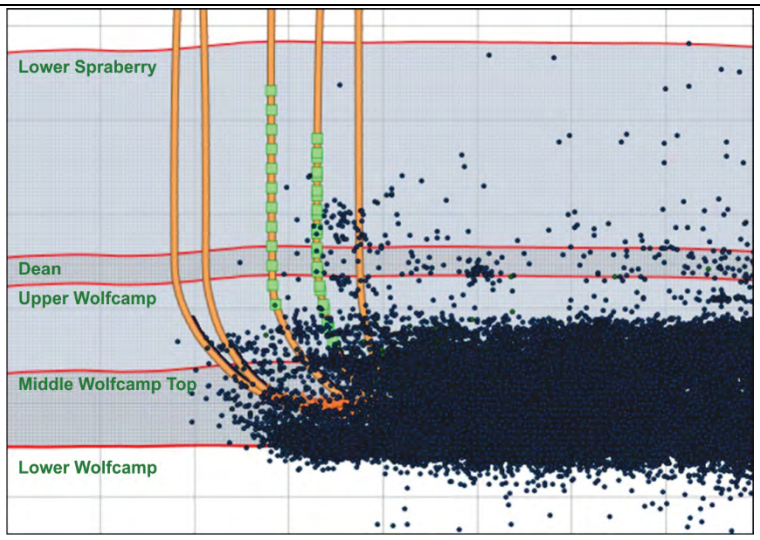

Figure 9: Side view of fracture height in the MW formation (color by formation).

MSM

Downhole MSM of the project was an involved process that required significant planning and coordination. Multiple vertical wellbores were dispersed throughout the 11-well pad, but only one well was suitable for use as a monitor well for the downhole geophones. To minimize background noise in a monitor well, all open perforations should be isolated with a bridge plug so there is only non-perforated pipe for the geophone monitoring. Existing perforations can produce gas bubbles, which result in high background noise that can interfere with the geophone's ability to detect the microseismic events. In addition to the vertical geophone arrays, a horizontal array was deployed in a horizontal well in the middle of the pad (Figure 3). The geophones were tractored into the well and then pulled back toward the heel during the offset well completions. This horizontal array was continually positioned directly across from the offset completion interval to help minimize the listening distance, reduce uncertainty, and minimize the observation well bias of the microseismic activity. The multiple-array setup provided excellent coverage across most of the pad at all times and delivered high-quality results. **Figure 10** shows an example of one fracturing stage, which provides some insight into the fracture geometry generation. Created fracture half-lengths of more than 900 ft and total fracture heights of 1,000 ft were observed. Fracture event clouds greater than 500-ft wide were also observed during some fracturing stages. This is not the effective propped fracture geometry but most likely closer to the created SRV.

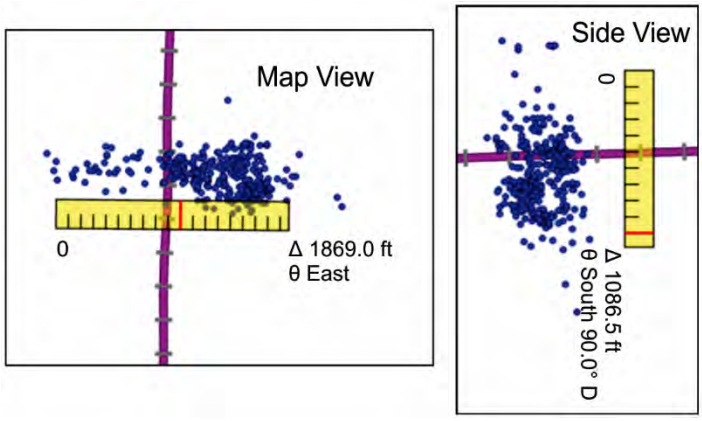

Figure 10: Example of fracture geometry (fracture length and height).

Representative Fracture Geometry from MSM

Typical fracture geometry is based on the results of representative stages, which were minimally affected by artifacts of the measurement [5], [6] and exhibit high data confidence. Some stages were not considered representative because they were pumped simultaneously with another stage; therefore, events attributed to those stages could actually be associated with their respective co-stimulated stage. **Figure 11** shows such an example. The MSM events (in the red oval) were located between the two treatment wells and could be assigned to either well because the completions were conducted during the same time period (two fracturing crews). Manual separation of the events was the only option at the time of the study, which extended the time necessary to deliver the final analysis. New processing techniques and algorithms have since been developed to address complex data sets acquired during multiwell zipper fracturing completions and have significantly decreased the post-completion processing time.

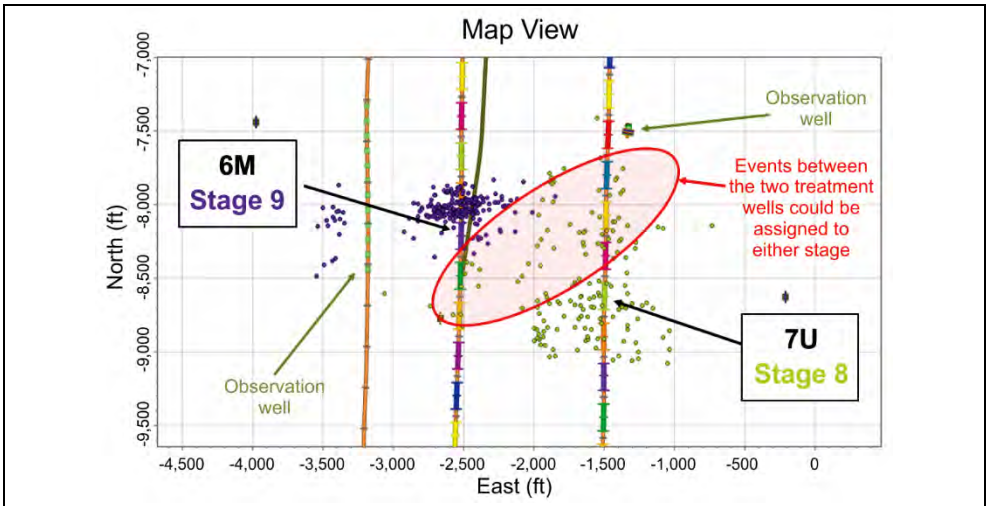

Figure 11: Map view of MSM events from simultaneously stimulated stages on Wells 6M and 7U.

Vertical coverage for the UW laterals extends from the top of the LW to the lower Spraberry formation, but based on the principles of Stokes' law and the use of low-viscosity fluid, proppant distribution beyond the Dean formation is not expected. For the MW wells, fractures extend from the top of the LW to the top of the lower Spraberry formation, although as with the UW laterals, the low-viscosity fluid selection suggests upward proppant placement was likely confined to the top of the LW formation. Therefore, proppant presumably was not distributed into the lower Spraberry and Dean layers. Some LW stages extended farther downward into the LW formation, and proppant was probably able to reach these depths. **Figure 12** shows the average height growth for each lateral relative to the perforation depth, respectively. The maximum fracture height was typically reached early during treatments according to the microseismic analysis. This relationship is consistent across all the project wells. **Figure 13 and Figure** 14 provide examples of the typical time/growth relationship for an UW and MW well, respectively.

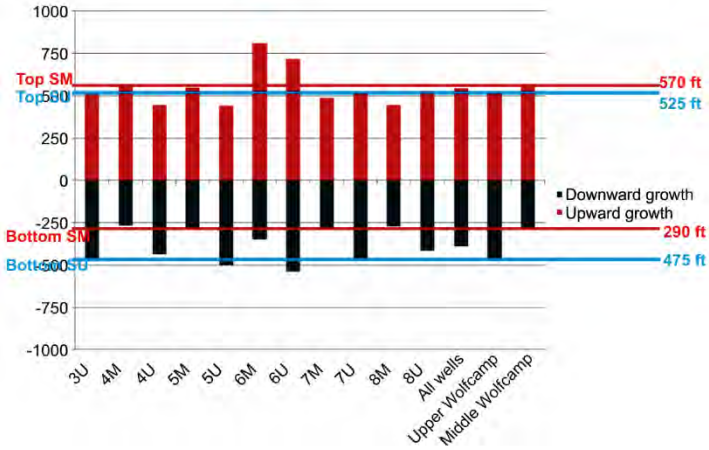

Figure 12: Average MSM height growth for all wells.

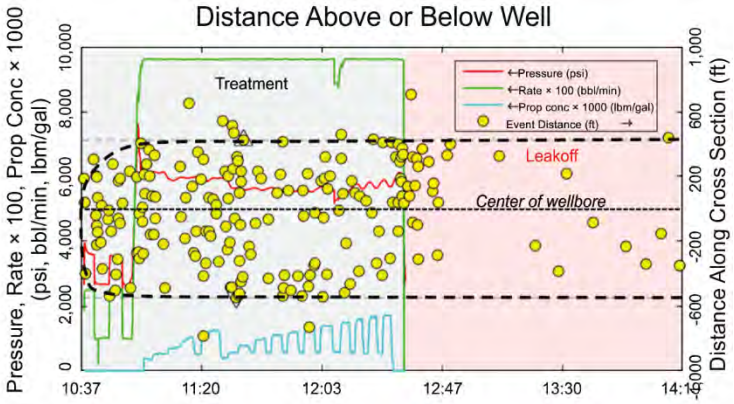

Figure 13: Example of typical fracture height and time relationship, Well 5U.

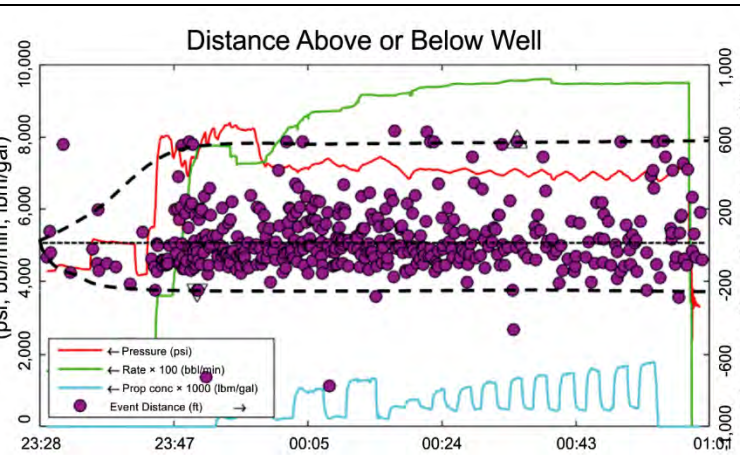

Figure 14: Example of typical fracture height and time relationship, Well 7M.

Perforation Cluster Design Comparison

Cluster count per stage varied between three vs. five clusters (entry points) per stage, and cluster spacing varied at 53 or 90 ft along the Well 4U and 7U laterals to determine whether these factors affected the created fracture geometry. Microseismic results can provide insight on additional far-field effects, such as azimuth and geometry

measurements, but near-wellbore (NWB)-related conclusions, such as cluster efficiency and fluid distribution, are often indeterminate or have a low degree of certainty because of the inherent limitations of event location near the wellbore and measurement artifacts. A NWB monitoring technology, such as fiber optics, can provide real-time temperature and acoustic measurements, which can provide accurate NWB fluid distribution. Based on the acquired microseismic data, the varying perforation cluster count and spacing had no discernible effect on the fracture geometry of the test wells vs. the standard completions on the other wells in the study. **Figure 15 and Figure** 16 show an example, in which fracture growth behavior and resulting geometry appear similar across the entire Well 4U lateral and are independent of the cluster design and number of entry points. While this is also likely true for the Well 7U lateral, the location of the MSM observation wells relative to the cluster design variations prevents a more definitive conclusion. **Figure 17** shows the Well 7U microseismic data and cluster design variation points.

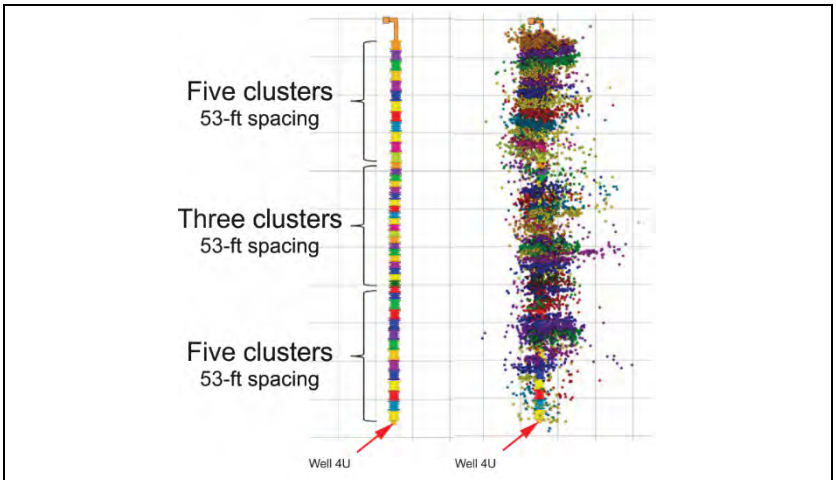

Figure 15: Perforation design and resulting fracture geometry on Well 4U.

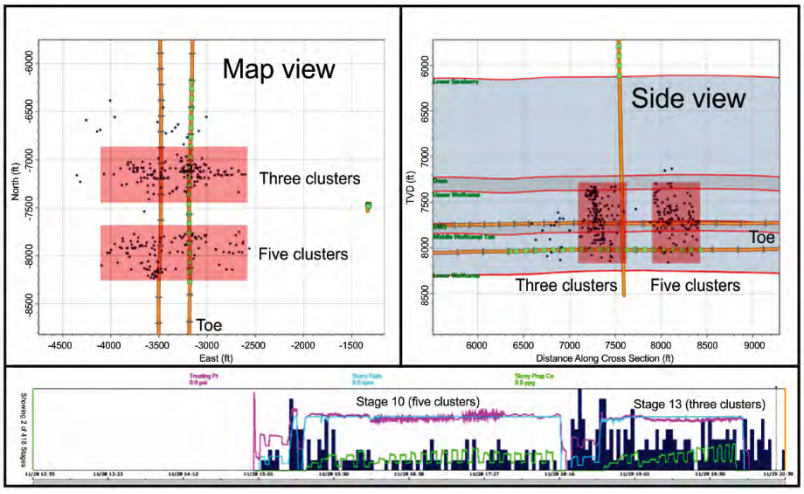

Figure 16: Comparison of Well 4U Stage 10 (five clusters) and Stage 13 (three clusters).

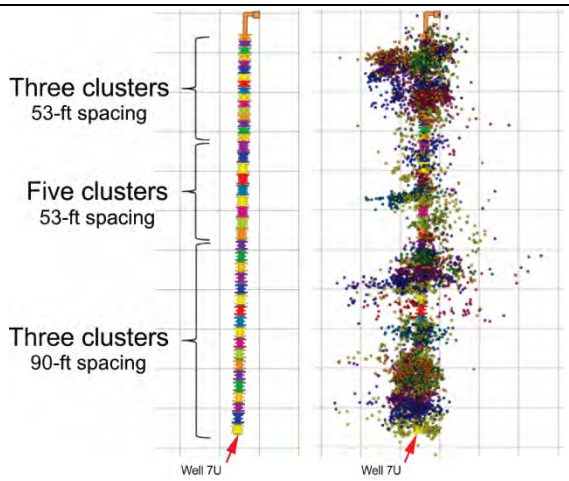

Figure 17: Well 7U perforation design and resulting fracture geometry.

Fracture Azimuth and Complexity

Figure 18 shows the primary and secondary azimuths for select stages. **Figure 19** shows charted azimuth measurements for all stages of the 11 wells. The primary fracture azimuth is consistent among all wells and at N76°E is oblique to the north-south lateral orientation. Most stages of the 11 wells have a clear, strong secondary azimuth of approximately N46°W and a relatively wide event-cloud width of 535 ft **(Figure 20),** which in conjunction suggest an overall moderate degree of fracture complexity was induced. Given the pervasive presence of the secondary azimuths and their rapid population after treatments began, a small differential between the degree of the maximum and minimum principal horizontal stress directions in this region is likely. This would allow fractures to readily propagate along the minimum stress trend. During some stages, the primary azimuth displays a more east-west direction, and no discernible secondary azimuth is observed **(Figure 21).** For these stages, complexity is probably low, although it is possible some slight NWB complexity is present.

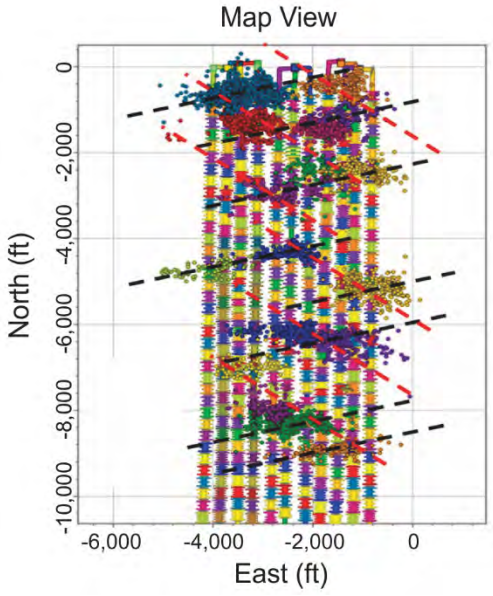

Figure 18: Map view of primary (black) and secondary (red) azimuths of selected project stages.

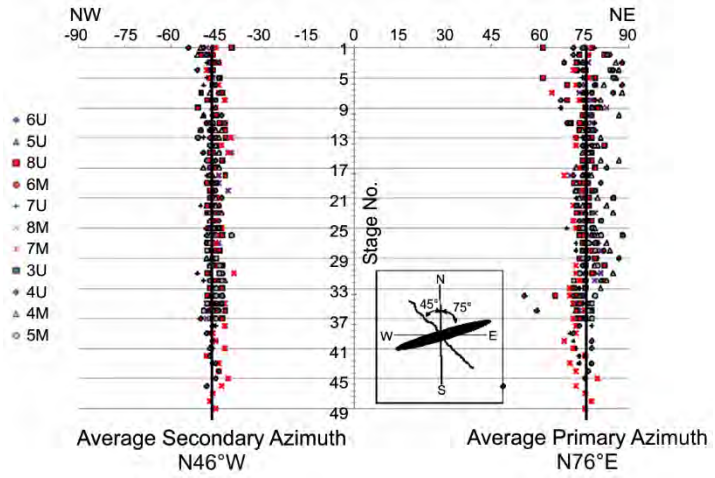

Figure 19: Primary and secondary fracture azimuths for all stages.

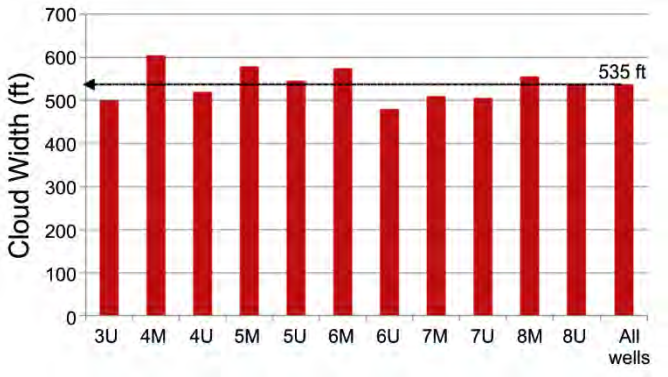

Figure 20: Average event-cloud width measurements for all wells.

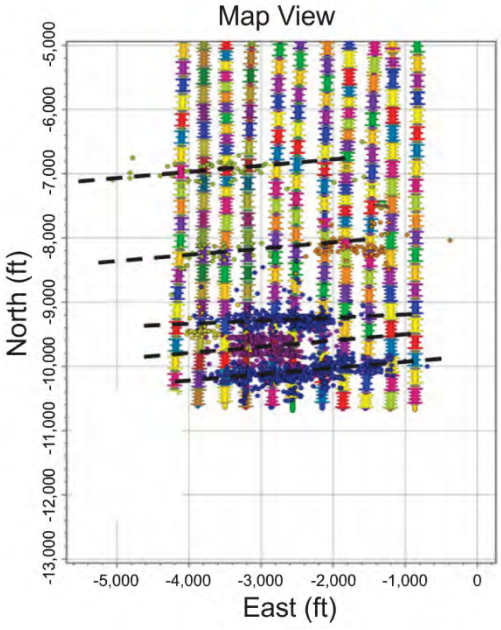

Figure 21: Map view of low complexity stages.

Completing the UW wells before the MW laterals might have affected certain aspects of the stimulation. Slightly wider event clouds were measured for the MW wells, and fracture gradients were generally higher during the MW stages compared to the UW stages **(Figure 22).** These findings might be associated with the MW fractures interacting with the previously created fractures of the UW project wells, although it is possible stress-shadowing occurred between MW stages, as heel-ward cloud movement accompanied the increased fracture gradients during most stages of this well (**Figure 23,** Stage 6 blue MSM events). Toe-ward microseismic activity between stages could be caused by leaking fracturing valves or continued microseismicity caused by leakoff from the previous fracturing stage (Figure 23, yellow MSM events overlapping Stage 4).

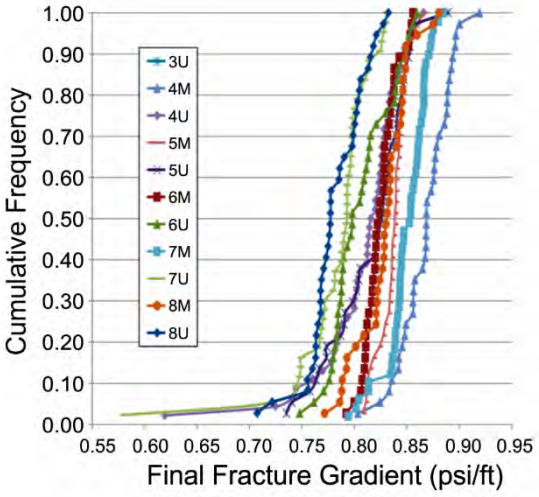

Figure 22: Final fracture gradients, all wells.

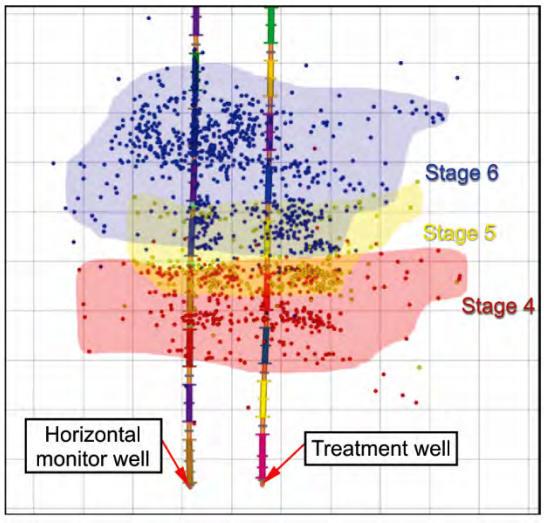

Figure 23: Interaction between adjacent stages, Well 5U Stages 4, 5, and 6.

Fracture half-lengths for the 11 wells range from 555 to 1,090 ft, with an average of 830 ft **(Figure 24).** Similar fracture extension exists between most formations, from the Dean to the bottom of the MW 2, but shorter fracture lengths in the LW and upper portion of the lower Spraberry are present **(Figure 25).** The maximum fracture half-length appears to have been reached approximately 60 minutes after the injections began. Only incremental growth was observed beyond this period. **Figure 26 and Figure** 27 show an example of this relationship for an UW and MW well.

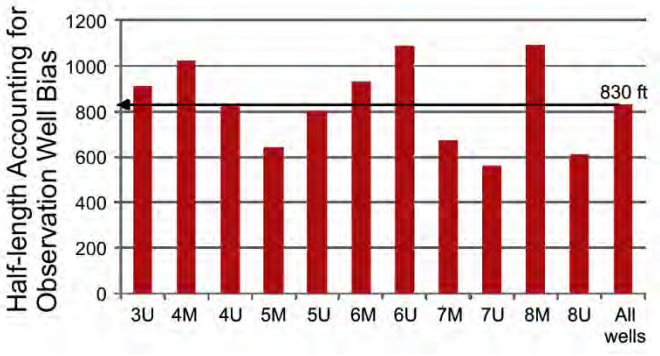

Figure 24: Average fracture half-length (ft) per well.

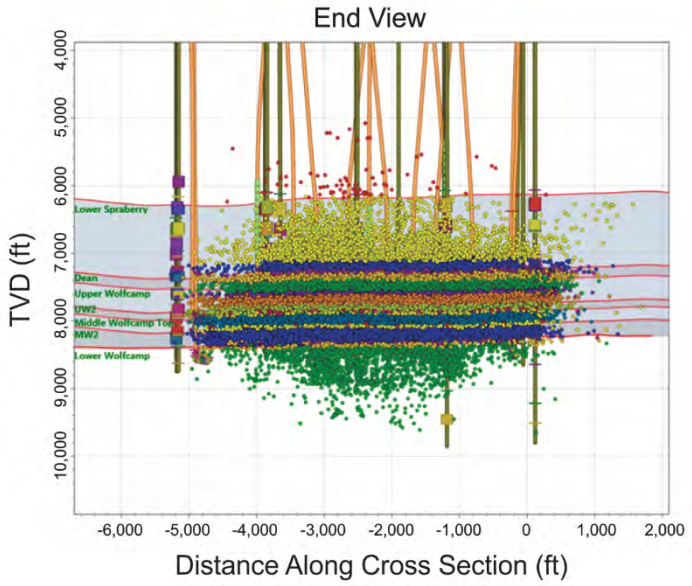

Figure 25: End view (gun barrel view) of all stages colored by formation.

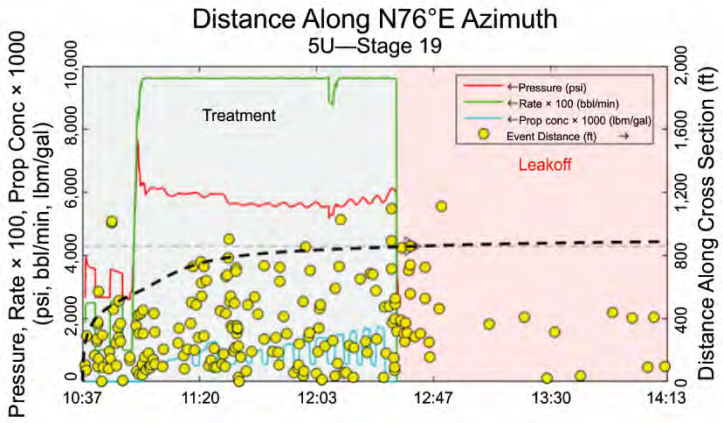

Figure 26: Example of fracture length and time relationship, Well 5U Stage 19.

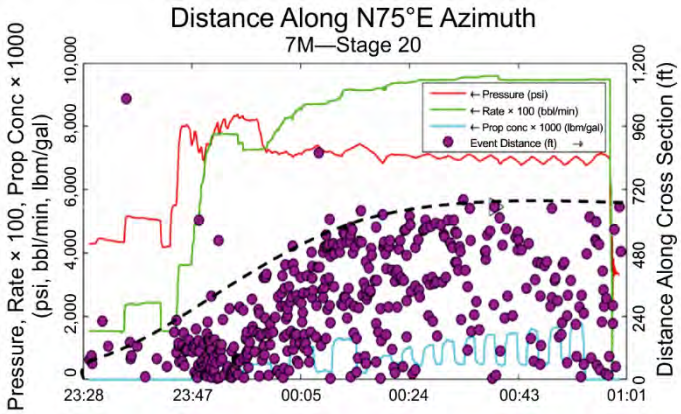

Figure 27: Example of fracture length and time relationship, Well 7M Stage 20.

Downhole Deformation Measurements (Tiltmeters)

The vertical monitor geophone array included a hybrid string of downhole tiltmeters [7], [8], [9]. The bottom of this toolstring was located approximately 1,500 ft above the uppermost lateral completion. The downhole tiltmeters were not intended to measure fracture height because the tools did not straddle the completion zone but were instead used to measure whether a hydraulic fracture actually extended upward past the toolstring array. The results showed only the lowermost tiltmeter indicated slight deformation of the reservoir rock during the completion (measured in microradians). This indicates that the hydraulic fractures generated during the completion did not propagate upward past the tiltmeter array. This means a hydraulic fracture was generated somewhere below the toolstring, which caused small vertical rock deformation at the leading edge of the upward growing fracture.

The tiltmeter records the magnitude of deformation (tilt) in microradians. It was concluded that the hydraulic fracture was somewhere below the tool's true vertical depth (TVD) and did not extend to a shallower depth beyond the array. Recorded responses are shown in **Figure 28 through Figure** 30**,** in which the lowest tiltmeter is displayed in white. **Figure 31** shows the correlated microseismic results from these stages, which support the downhole microdeformation conclusions.

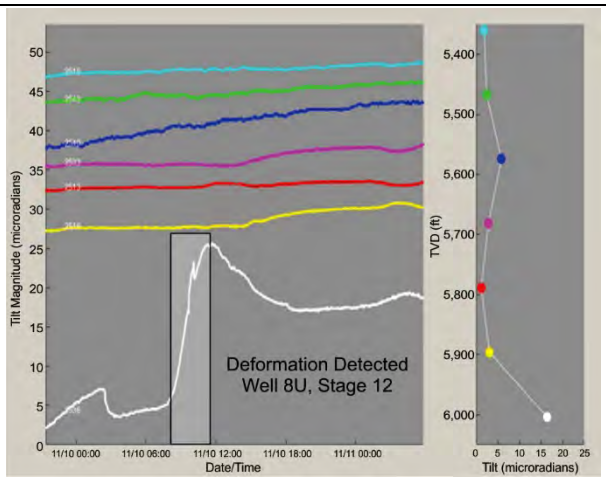

Figure 28: Deformation detected during Well 8U Stage 12.

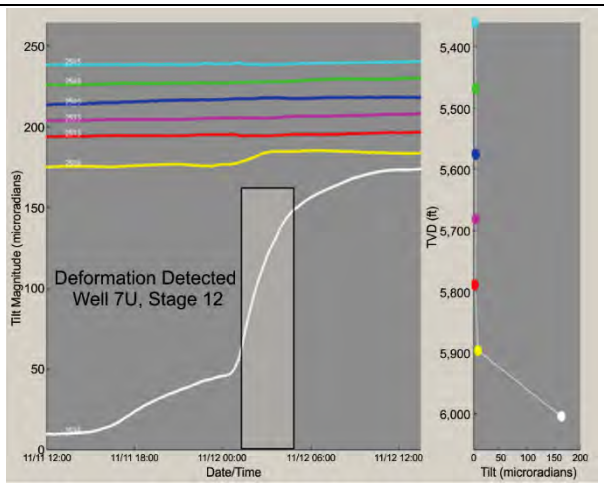

Figure 29: Deformation detected during Well 7U Stage 12.

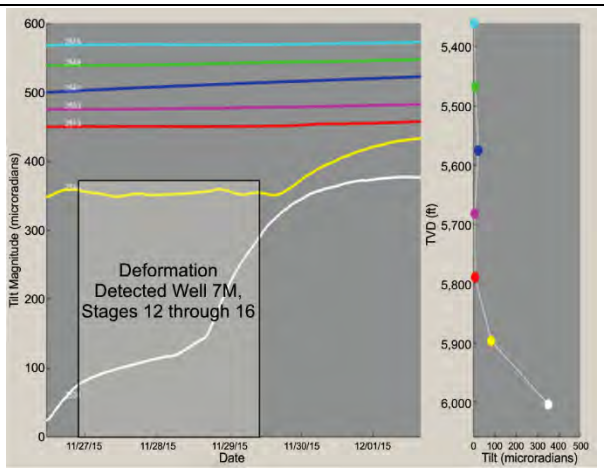

Figure 30: Deformation detected during Well 7M Stages 12 through 16.

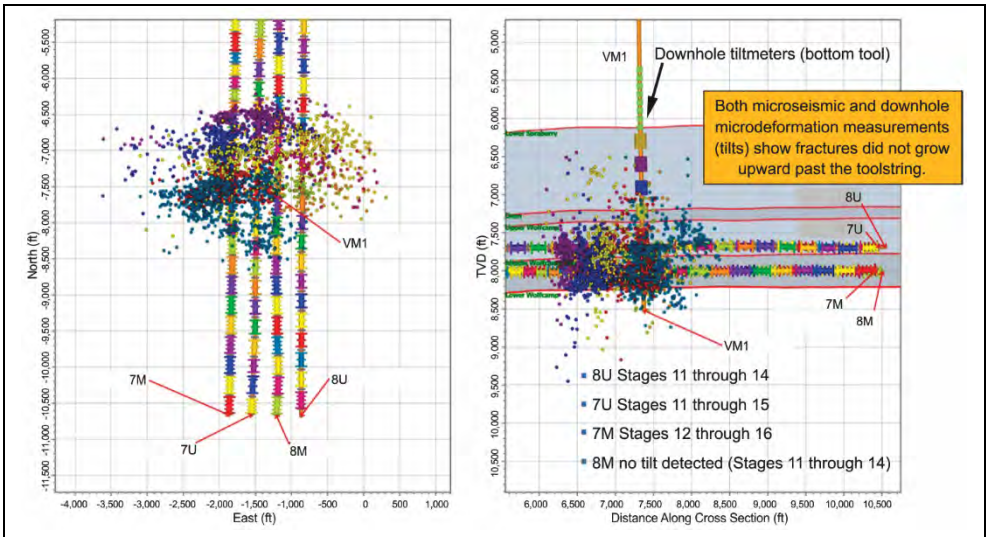

Figure 31: Correlating microseismic measurements during tiltmeter deformation detection.

MSM Data Relative to the "Slant Well" Post-Fracturing Whole Core

Two sections of openhole core were cut in Well 6SW (slant well) after the completion of the pad wells to provide a TVD/measured depth (MD) reference to previously recorded Well 6U and 6M events. Approximately 400 ft of core was cut adjacent to Stages 22 through 24 of Well 6U, and another 200 ft was cut across from Well 6M Stages 14 and 15. Events from these stages were then compared to the known TVDs along the two core portions of the 6SW slant well to further characterize fracture growth. Results indicate that the UW events are less planar and more dispersed than the MW events. The slight decrease in planar growth could be caused by the lithological properties in the UW. It is possible that there is a higher concentration of natural fractures in the UW vs. MW. Induced stresses related to the completion sequencing (UW wells stimulated before the MW wells) could have also contributed to the differing growth pattern. **Figure 32 through Figure** 34 show the microseismic results from Well 6U Stages 22 through 24 and Well 6M Stages 14 and 15 vs. the adjacent core cuts along Well 6SW.

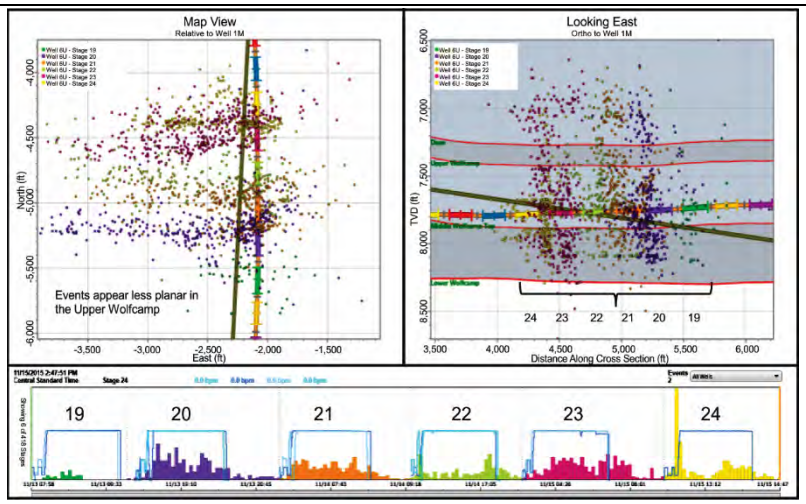

Figure 32: Core cut along Well 6SW adjacent to Well 6U Stages 19 through 24.

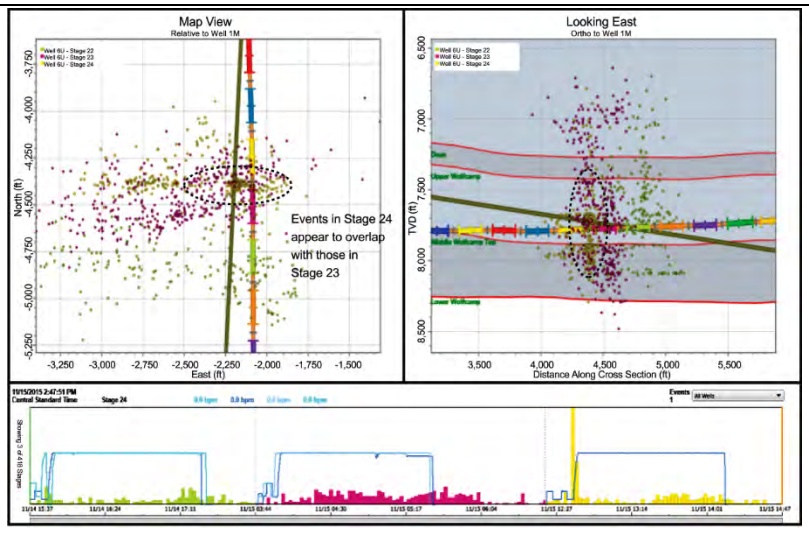

Figure 33: Core cut along Well 6SW interval adjacent to Well 6U Stages 22 through 24.

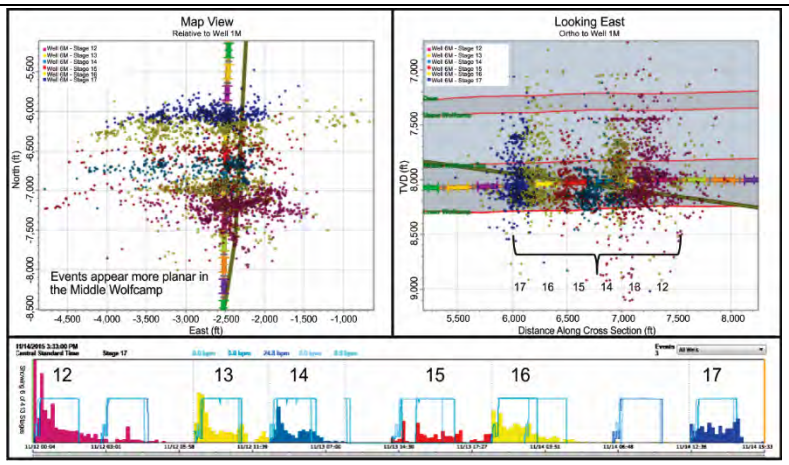

Figure 34: Core cut along Well 6SW interval adjacent to Well 6M Stages 12 through 17.

Observations and Conclusions

The following conclusions are a result of this work.

- Fracture geometry is relatively consistent for all 11 wells; however, some localized differences might exist (offset production, interaction with previous fractures, etc.).
- Primary fracture azimuth is N76°E and secondary azimuth is N46°W.
- A moderate overall degree of complexity with additional exposed surface area in the secondary direction was likely achieved.
- Hydraulic fractures did not extend vertically upward beyond the downhole tiltmeter array (~1,500 ft above the UW laterals).
- Additional fracture complexity was possibly the result of back-to-back completions (zipper fracturing) and stress-shadowing effects.
  - Constructive interaction existed between stimulations
  - Fractures in the LW were relatively contained because of UW completions
- Generally, most of the fractures appear symmetric or show slightly asymmetric fracture growth (because of vertical offset production).
- Timing between completion sequencing does not appear to make a difference (based solely on microseismic data) if the completion
  - Begins immediately with alternating stages between wells (zipper fracturing)
  - Begins by pumping the first five stages on one well and then alternating stages (zipper fracturing)
- The optimum number of perforation clusters per stage and cluster spacing was indeterminate, based on only the microseismic data, because of
  - Difficulty establishing a baseline for the DOE
  - Microseismic measurement artifacts
  - Completion interval variations (UW and LW)
- NWB diagnostics (fiber optics) are necessary to determine NWB fluid distribution and cluster efficiency.

Acknowledgements

The authors thank the HFTS consortium members for their patience during the completion of the MSM analysis and Laredo Petroleum, Inc. for hosting the test site for this project.

References

[1] Staples, Evan, Patrick Perfetta, Jamal Sandarusi, and Jennifer Adams. "Exploration Through Early Appraisal of the Horizontal Wolfcamp Play in the Ozona Area, Southern Midland Basin." URTEC-2154046-MS presented at the Unconventional Resources Technology Conference, San Antonio, Texas, USA, 20-22 July 2015.

[2] Friedrich, Mickey and Gene Monson. "Two Practical Methods to Determine Pore Pressure Regimes in the Spraberry and Wolfcamp Formation in the Midland Basin." URTEC-1582132-MS presented at the Unconventional Resources Technology Conference, Denver, Colorado, USA, 12-14 August 2013.

[3] Courtier, James, Danny Gray, Michael Smith, Neil Stegent, James Carmichael, Magdy Hassan, and Jordan Ciezobka. "Legacy Well Protection ReFrac Mitigates Offset Well Completion Communications in Joint Industry Project." SPE-181767-MS presented at the SPE Liquids-Rich Basins Conference – North America, Midland, Texas, USA, 21-22 September 2016.

[4] Mayerhofer, Michael J., Elyezer Lolon, Norman Raymond Warpinski, Craig L. Cipolla, Douglas W. Walser, and Claude Michael Rightmire. "What is Stimulated Rock Volume?" SPE-119890-MS presented at the SPE Shale Gas Production Conference, Fort Worth, Texas, USA, 16-18 November 2008.

[5] Warpinski, Norm. "Microseismic Monitoring: Inside and Out." *Journal of Petroleum Technology* 61, no. 11 (November 2009): 80-85. SPE-118537-PA.

[6] Cipolla, Craig L., Mark Gavin Mack, Shawn C. Maxwell, and Robert C. Downie. "A Practical Guide to Interpreting Microseismic Measurements." SPE-144067-MS presented at the North American Unconventional Gas Conference and Exhibition, The Woodlands, Texas, USA, 14-16 June 2011.

[7] Wright, C.A., E.J. Davis, G.M. Golich, J.F. Ward, S.L. Demetrius, W.A. Minner, and L. Weijers. "Downhole Tiltmeter Fracture Mapping: Finally Measuring Hydraulic Fracture Dimensions." SPE-46194-MS presented at the SPE Western Regional Meeting, Bakersfield, California, USA, May 10-13 1998.

[8] Warpinski, N.R., M.J. Mayerhofer, E.J. Davis, and E.H. Holley. "Integrating Fracture Diagnostics for Improved Microseismic Interpretation and Stimulation Modeling." URTEC-1917906-MS presented at the Unconventional Resources Technology Conference, Denver, Colorado, USA, 25-27 August 2014.

[9] Fisher, Mark Kevin and Norman Raymond Warpinski. "Hydraulic Fracture-Height Growth: Real Data." SPE-145949-MS presented at the SPE Annual Technical Conference and Exhibition, Denver, Colorado, USA, 30 October–2 November 2011.

Appendix A: Representative MSM Graphics

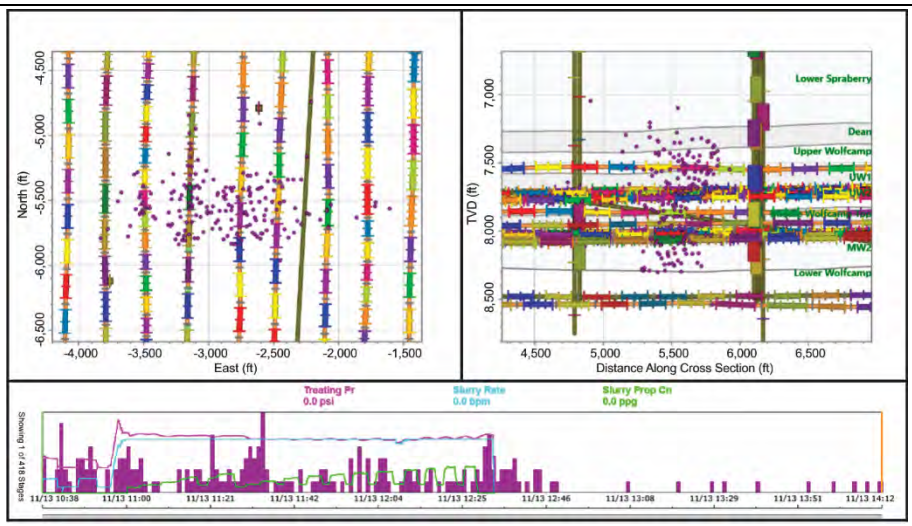

Figure A-1: Map and lateral side views of typical Well 5U geometry, Stage 19.

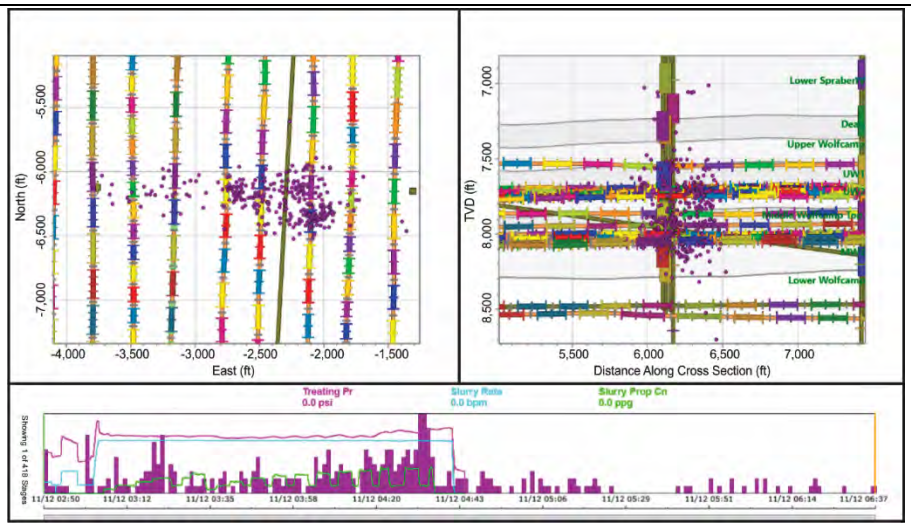

Figure A-2: Map and lateral side views of typical Well 6U geometry, Stage 17.

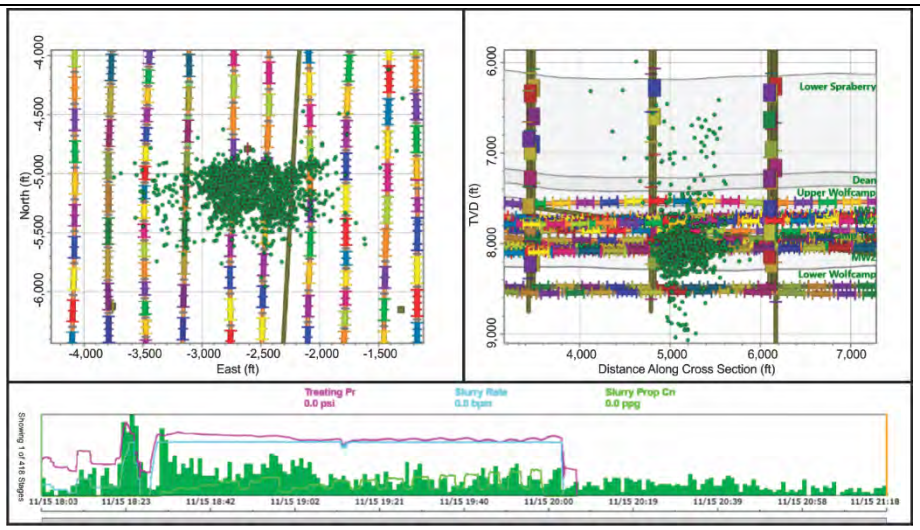

Figure A-3: Map and lateral side views of typical Well 6M geometry, Stage 20.

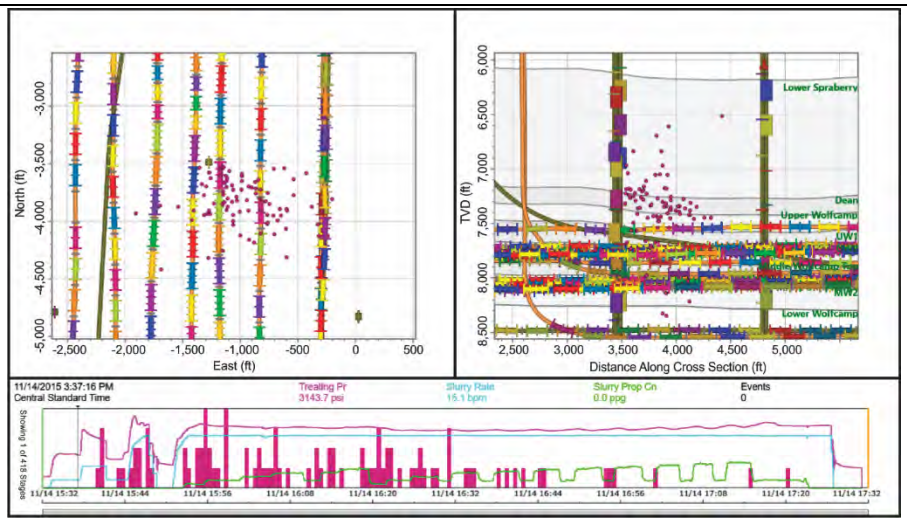

Figure A-4: Map and lateral side views of typical Well 8U geometry, Stage 25.

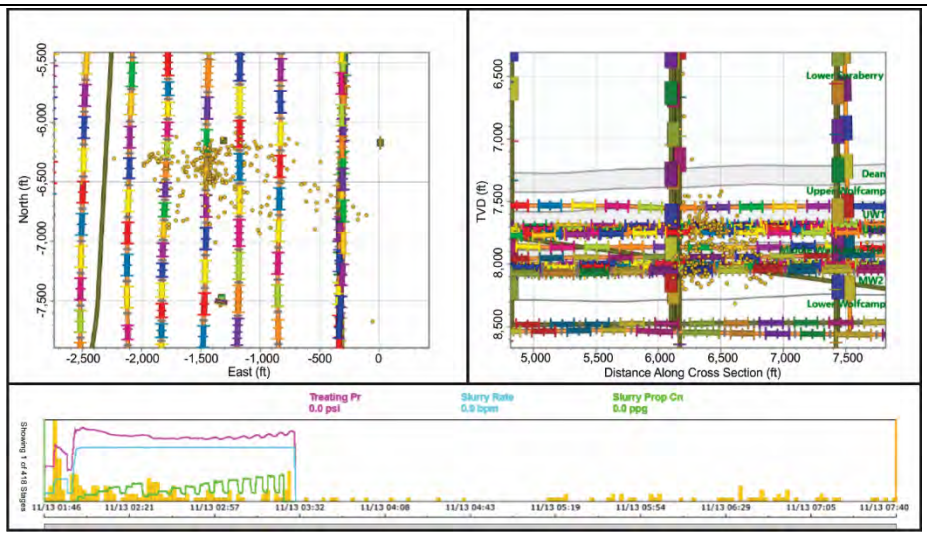

Figure A-5: Map and lateral side views of typical Well 7U geometry, Stage 16.

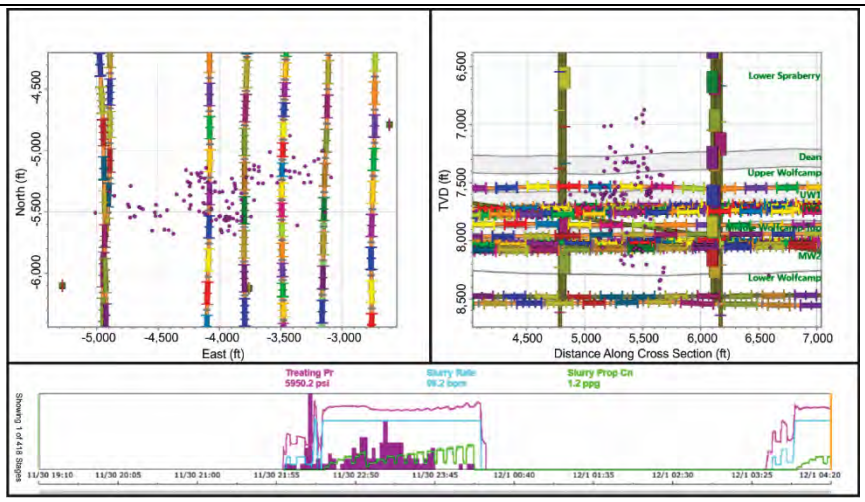

Figure A-6: Map and lateral side views of typical Well 3U geometry, Stage 20.

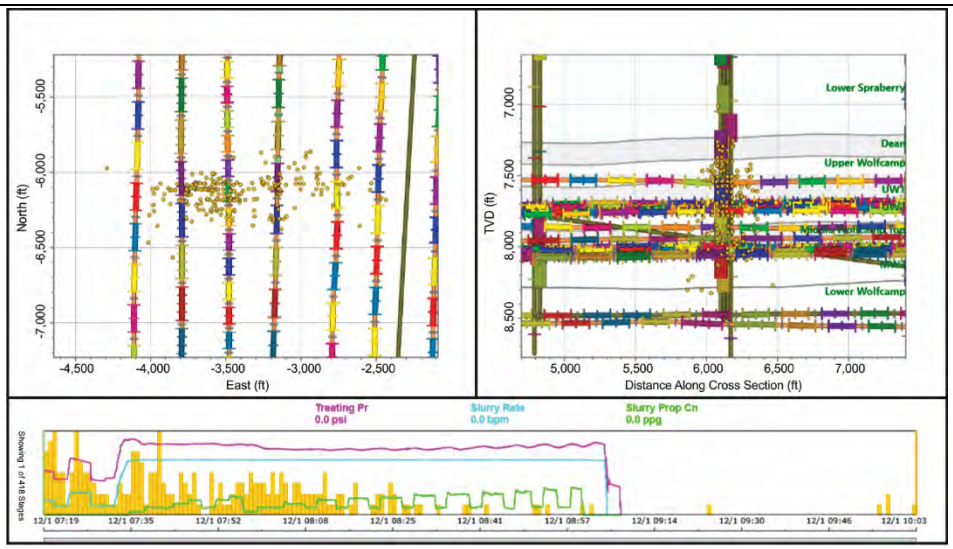

Figure A-7: Map and lateral side views of typical Well 4U geometry, Stage 19.

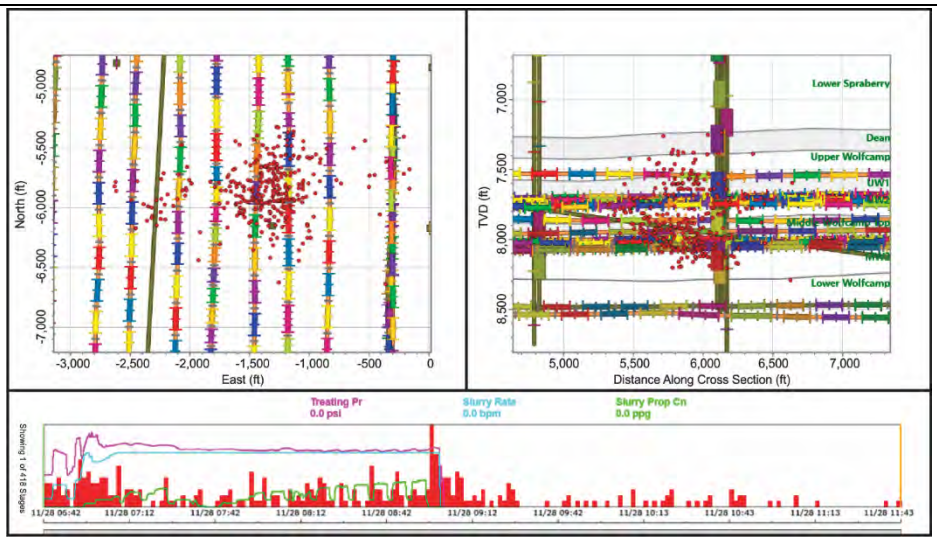

Figure A-8: Map and lateral side views of typical Well 8M geometry, Stage 17.

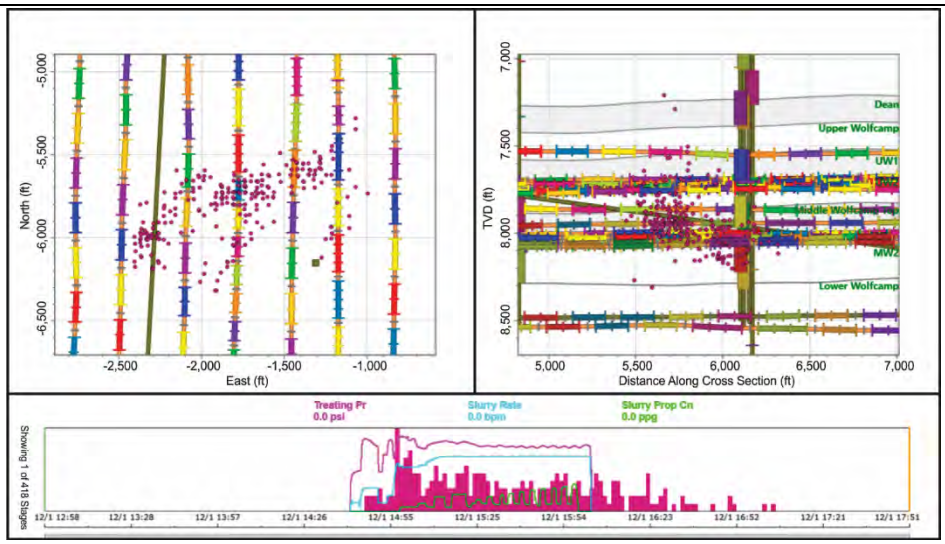

Figure A-9: Map and lateral side views of typical Well 7M geometry, Stage 22.

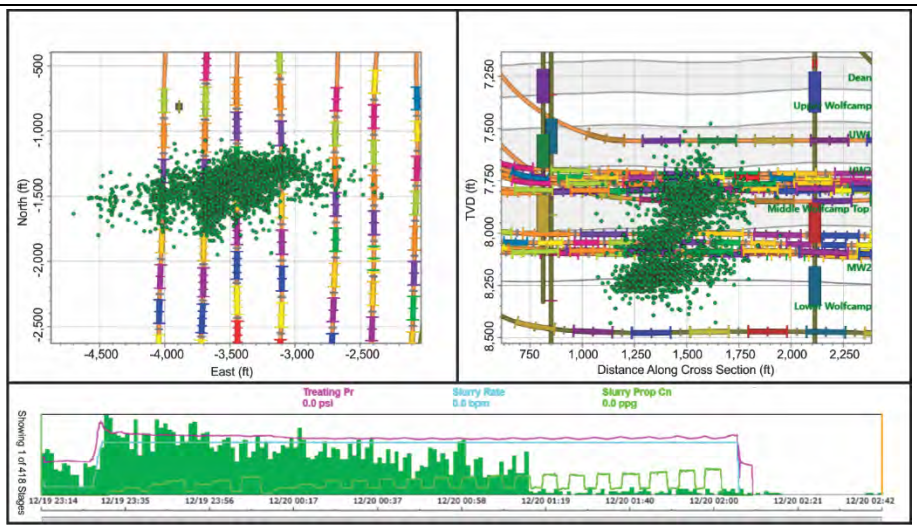

Figure A-10: Map and lateral side views of typical Well 4M geometry, Stage 33.

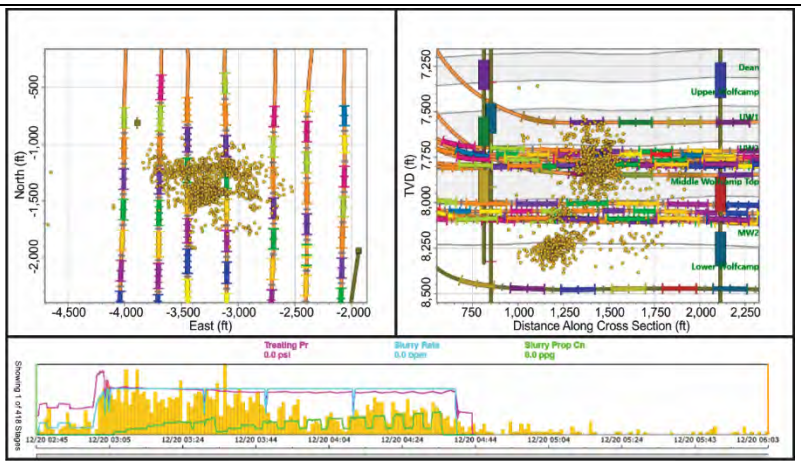

Figure A-11: Map and lateral side views of typical Well 5M geometry, Stage 33.

Appendix B: MSM QA

The key QA components of this analysis are the position of the tools and the accuracy of calculations and/or inversions. These two factors can influence the accuracy of the results and ultimately provide a better understanding of the created fracture geometry.

The first QA key component is the position of the tools used to map the project. Ideally, the array should be deployed as near to the target as possible, in both distance and depth, to minimize error and increase the signal-to-noise ratio (SNR). All treatment and observation laterals were landed in either the UW or MW with a parallel lateral spacing for wells at approximately the same TVD of 600 ft. The 11 wells were divided among three pads. The observation wells used during this project included the following:

- Well 5M, which is located between the Well 4U and 5U laterals
- Well 3U, which is the westernmost lateral of the three treatment pads, with Well 4M directly east of it
- Well 6U, which is between the Well 5U and 4U laterals
- Vertical monitor well, located approximately equidistant (at 100 ft) from Wells 7U and 7M

Table B-1 shows the location of the monitor wells relative to the completion wells along with the monitored fracturing stages.

Phase No.	Treatment Well (Total Stages)	Observation Wells					
		5M Horizontal	5M Vertical 1	5M Vertical 2	6M	3U	Vertical Monitor Well
1	5U (37)	1 through 32		33 through 37			1 through 37
	6U (37)	1 through 32		33 through 37			1 through 37
	6M (37)	1 through 28		29 through 37			1 through 37
	8U (37)	1 through 37					1 through 37
	7U (43)	1 through 37		38 through 43			1 through 43
2	3U (37)	1 through 31	32 through 37				1 through 37
	4U (46)	1 through 29	30 through 46				1 through 46
	8M (37)	1 through 34	35 through 37				1 through 37
	7M (49)	1 through 29	30 through 49				1 through 49
3	4M (37)				1 through 37	1 through 37	
	5M (37)				1 through 37	1 through 37	

Table B-1: Completion order, fracturing stages monitored, and observation wells.

A dual-receiver-array configuration was used throughout this project by means of four different toolstrings:

- An eight-level fracture-mapping hybrid receiver array (16 double-stacked microseismic tools and eight tiltmeters)
- An 18-tool, 12-level horizontal receiver array
- Two 24-tool, 12-level vertical arrays

The hybrid array in Well 170P recorded data during all stages of the first two pads. To complete the dual-array configuration for these pads, a horizontal array was placed in the nearby Well 5M. An optimum listening distance was achieved by moving the array heel-ward during the Pad 1 and 2 completions as the stages of each zipper fracturing sequence progressed. The array in Well 5M was pulled to a vertical position during the heel-most stages of all wells in Pads 1 and 2, except for the Well 8U completion. All Well 8U stages were monitored by means of a horizontal array position. After the completion of Pad 2, the array in Well 5M was removed. Pad 3 (Wells 5M and 4M zipper fracturing) was monitored using two vertical arrays—one deployed in Well 6M and one in Well 3U.

All vertical arrays were positioned above the treatment laterals because the vertical observation well was previously produced at multiple intervals across the Wolfcamp, Dean, and Spraberry formations, and the vertical arrays placed in the treatment laterals could only be lowered to just above the kickoff point within the vertical portion of the laterals. The bottom tool for the hybrid array was located at the top of the Spraberry formation, which was an ideal position for the tiltmeters because any extension into the Spraberry would be detected. While the other vertical arrays were not in an optimal position, they were reasonably close to the treatment wells and within the target zone. Therefore, increased event location uncertainty resulting from toolstring positioning is probable but not extensive.

The bottom tools of the vertical array placed in Wells 4M, 6M, and 5M were at approximately the same TVD, with Wells 4M and 6M in the middle of UW 1 and Well 5M at the top of UW 2. A shallower toolstring position was required for the vertical array in Well 3U because of its slightly shallower landing depth. For this array, the bottom tool resided near the base of the lower Spraberry 3L.

Individual microseismic sondes of 5.03-in. length and 2.50-in. diameter were composed of six OYO DS-250 15-Hz geophones—two X, two Y, and two Z—to internally stack the signal for single-channel data. Receivers were double stacked (i.e., two sondes per level) to enhance the SNR, decrease attenuation, improve hodogram linearity, and clarify phase arrival times. To obtain the total tilt vector, each tiltmeter contained two orthogonal sensors clamped between the microseismic tools on the same wireline. The arrays were configured using a varying number of flexible interconnects (30 m in length) depending on the number of levels in the toolstring (each level had one interconnect between it and the next level). The temperature limit of a DS-250 array is 275°F. Because the highest static temperature in the monitor well was well below this threshold, there were no tool failures caused by temperature restrictions. Microseismic data was sampled at 0.25-ms intervals and microdeformation data every 4 seconds.

During deployment, geophones rotate freely according to the localized torque. While the Z-axis of each sonde is aligned with the wellbore, the X and Y components can face in any direction perpendicular to each other. Tool orientation, or the direction of each tool component, is based on calibration points, as recorded by the array. Calibration points are audible events with known points of origin, such as an early event, a perforation shot, a string shot, a tubing-conveyed perforating (TCP) shot, a correlated surface vibe shot, or other mechanical source that produces a series of recordable P- and/or S-waves. During this project, the toolstring was oriented using perforation shots. Perforation-timing boxes were clamped to the perforation wireline and recorded the change in voltage during perforation detonation, thus providing a known calibration origin point in space and time. By calculating the compressional particle motion direction and angle from these events to a tool, the actual geophone locations were confirmed. Because the tiltmeters were coupled to the microseismic tools on the same wireline, they could be oriented at the same time using the same method.

Microseismic Velocity Model Optimization

The second key QA component is the accuracy of the velocity model used to analyze the microseismic data set. Anisotropic modeling [i.e., 3D vertical transverse isotropy (VTI) modeling] was used to accurately locate microseismic events produced from the three pad stimulations. With five components per layer, VTI modeling results in a more accurate Earth model of the area. This project used four VTI velocity models, each comprising 22 layers, in which the velocities delineate obvious changes in rock properties with depth **(Figure B-1).** It was initially developed with operator-provided Thomsen parameters, dipole sonic, and gamma ray data from an offset well. A forward modeling algorithm was used to calculate travel times and ray paths between grid points and the monitoring tools for every grid point in the model. This allowed each event to be located based on its P- and S-wave arrival times. Model optimization was accomplished by lowering the time residuals and minimizing the distance error between a known location and the inverted location. This model was optimized by analyzing the P- and S-wave arrival times of the stage perforation shots at the array. In conjunction with perforation timing, a very fast simulated annealing (VFSA) inversion algorithm was applied during post-processing until the time residuals and locations improved. Time residuals for the majority of the data matched the picked arrivals reasonably well. However, inconsistencies were greater for events located farther from the array or shallower than the wellbore because of a lack of reliable calibration points in these areas. Overall, the final time residuals fell within an acceptable range.

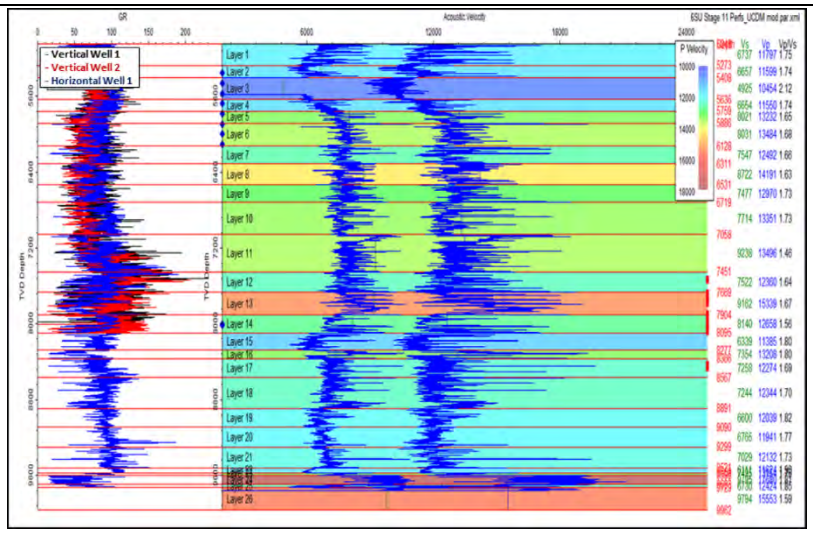

Figure B-1: Final VTI Velocity Model 1 used during Phase 1 and 2 stages.

Microseismic Data Quality

The overall quality of the microseismic data is moderate. Results include a final total of 128,405 events for all stages monitored—an increase of 30% over the real-time count of 4,271 events. Tiltmeters in the hybrid array functioned properly; therefore, any microdeformation activity at or above the bottom tilt tool would have been detected.

The microseismic event SNR ranged from 0 to 108, and microseismic events of average magnitude were imaged up to 4,500 ft from the toolstring. The point of crossover between the detection limit and the size of the largest events is considered the maximum viewing distance **(Figure B-2).** With longer distances, events should be of higher magnitude to be detected by the microseismic tools. The detection limit is inversely proportional to the noise level, increasing with lower ambient noise and decreasing with increasing noise levels. Background noise levels averaged approximately 1,800 nV, which is considered average. **Figure B-3** shows typical background noise levels during pumping.

Event-location error was calculated using 2D modeling, which consisted of three error "directions"—azimuth, radius (tool-to-event distance), and depth (elevation). The greatest component of uncertainty for the operator's pads is depth, with an average error of 49 ft. The average azimuthal uncertainty is 33 ft, and the average radial uncertainty is 47 ft. The depth error component was the largest of the three directions during this project because the vertical receiver arrays were placed well above the depth of the treatment laterals. Using vertical arrays that straddle the treatment lateral depths can minimize the error. Azimuthal error chords are displayed radially around the observation well as lateral error arcs, as they reflect the variations and uncertainties in the azimuth between the array and the microseismic events. Both distance- and depth-error bars associated with an event become longer as the time residual misfit increases. The size of the depth-error bar depends not only on the picked P- and S-wave arrival times but also on the relative position of the microseismic toolstring to the event location. Ideally, geophones should be located above and below the event location and as near to the target depth as possible to minimize depth error and increase the SNR.

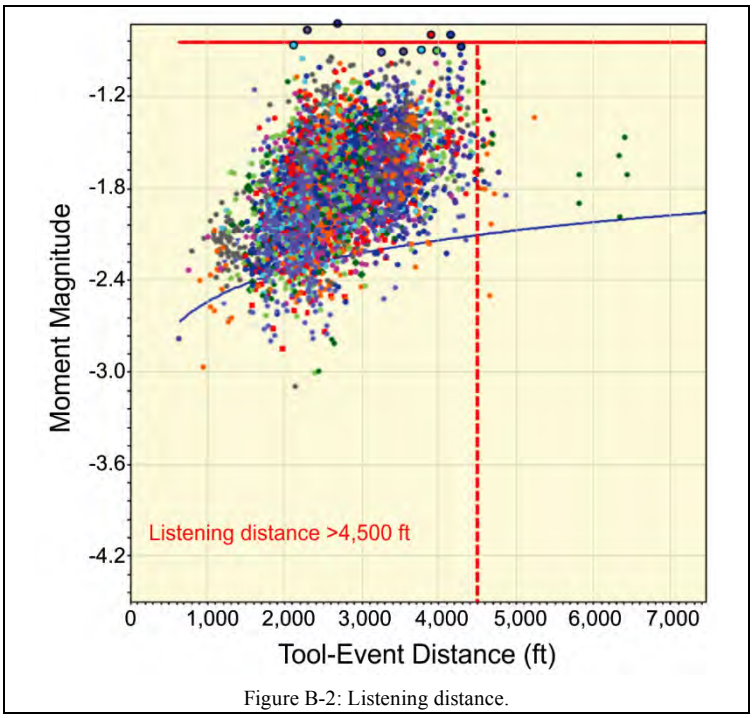

Figure B-2: Listening distance.

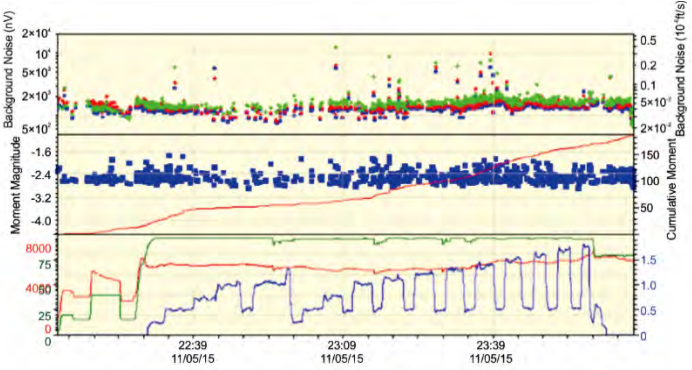

Figure B-3: Typical background noise levels.